Supporting Information

Biomimetic Reversible Heat-Stiffening Polymer Nanocomposites

Elvis Cudjoe[†], Shaghayegh Khani[†], Amanda E. Way[†], Michael J.A. Hore[†], Joao Maia[†*], Stuart J. Rowan[†,§,‡,*]

[†]*Department of Macromolecular Science and Engineering, Case Western Reserve University, 2100 Adelbert Road, Cleveland, Ohio 44106, USA.*

[§]*Institute for Molecular Engineering, The University of Chicago, 5640 South Ellis Avenue, Chicago, Illinois 60637, USA.*

[‡]*Department of Chemistry, The University of Chicago, 5735 S Ellis Ave, Chicago, IL 60637, USA.*

Experimental

Materials. Hydrochloric acid (HCl), sodium hydroxide (NaOH), sodium bromide (NaBr), sodium chloride (NaCl) and sodium hypochlorite (NaClO, 14.5% chlorine content) were purchased from Fisher Scientific. HyClone Earle's balanced salt solution (EBSS) was purchased from Thermo Scientific. 2-(2-(2-methoxyethoxy)ethoxy)ethyl acrylate was synthesized according to the literature.[39] Commercially available 2-(2-methoxyethoxy) ethyl methacrylate was passed through a basic alumina column before use. 2,2,6,6-tetra-methyl-1-piperidinyloxy (TEMPO), 2-bromoisobutyryl bromide, 2-(2-aminoethoxy) ethanol, Copper (I) bromide, *N,N,N', N'', N''*-pentamethyl diethylene triamine (PMDETA), phthalic anhydride, N-hydroxy succinimide (NHS), 1,3-diisopropyl carbodiimide (DIC) and triethylamine were purchased from Sigma Aldrich. Ultra-thin holey carbon-coated copper TEM grid and uranyl acetate were purchased from TED PELLA, inc. Sea tunicates (*Styela Clava*) were collected from floating docks in Warwick Cove Marina (Warwick, RI); tunicate mantles were obtained as previously described.[40]

Methods. The mechanical properties of the nanocomposites were characterized by dynamic mechanical analysis (DMA, TA instruments Model Q800). Tests were conducted using a film/fiber tension clamp or submersion clamp and temperature sweeps were performed at 0.1% strain, 0.01N Preload Force, and Force Track of 125%. Differential Scanning Calorimetry (DSC) were performed on a TA instruments Q2000. All samples were run under a flowing nitrogen atmosphere and were heated and cooled at a rate of 10 ºC/min through the temperature range of -80 to 80 ºC. Size Exclusion Chromatography (SEC) was performed on a Varian ProStar 210/215. THF was the eluent and run at a flow rate of 1 mL/min. The effect of hydrazine on the bromine terminus of the polymer was investigated by making a low molecular weight polymer and analyzing the end group

using a Bruker AUTOFLEX III Matrix Assisted Laser Desorption/Ionization (MALDI) mass spectrometer. α-Cyano-4-hydroxycinnamic acid and potassium trifluoroacetate were used as the matrix and doping salt respectively. CNCs were dispersed by ultra-sonication using a Q500 QSonica Ultrasonic processor at a 40% amplitude. Samples were freeze dried on a VirTis benchtop K lyophilizer. Titrations of the carboxylic acid groups on the CNCs were performed using an Accumet AR50 dual channel pH/ion/conductivity meter. FT-IR spectroscopy was performed on an Agilent Technologies Cary 600 series instrument over the range of 400 – 4000 cm^{-1}. Wide Angle X-ray Diffraction (WAXD) was obtained using a Rigaku S-MAX 3000 at a voltage of 45 kV and a current of 0.88 mA. Cu kα X-rays (λ = 0.1542 nm) were collimated to a final spot size of 0.7 mm. Transmission Electron Microscopy (TEM) was performed on a FEI Technai F30 at 300 kV to observe the CNC morphology on TEM grids stained with 2wt% uranyl acetate. AFM studies were carried out with a Bruker Multimode 8 in tapping mode using a silicon cantilever tip (scanasyst-air model, veeco) with a nominal spring constant of 0.4 N/m. The samples were drop-casted on freshly cleaved mica which was pre-coated with Poly-L-Lysine.

Synthesis of Carboxylic acid functionalized CNCs

Carboxylic acid functionalized tunicate CNCs (*t*-CNC-COOH) were synthesized according to our previously published procedure.[40] Determination of functional group content on *t*-CNC-COOH was conducted via conductometric titration. The charge density of *t*-CNC-COOH was 954 mmol/kg.

Synthesis of N-(2-(2-Bromoisobutyryl)ethoxy)ethyl phthalimide (1)

N-(2-(2-bromoisobutyryl)ethoxy) ethyl phthalimide was synthesized according to previously published literature[38] and isolated as a yellow oil in a 79% yield. ^{1}H NMR (600 MHz, $CDCl_3$): δ (ppm) 1.86 (s, 6H), 3.73 (t, 2H), 3.78 (t, 2H), 3.90 (t, 2H), 4.28 (t, 2H), 7.73 (m, 2H), 7.84 (m, 2H). ^{13}C NMR (150.8 MHz, $CDCl_3$): δ (ppm) 30.6, 39.9, 55.3, 64.8, 67.8, 68.1, 123, 132.2, 133.8, 168, 171.1.

Preparation of Phthalimide end capped Poly(2-(2-(2-Methoxyethoxy)ethoxy)ethyl methacrylate) ($POEG_3A$)

Cu(I)Br (2.6 mmol), PMDETA (2.6 mmol) and a dry stir bar were added to a dry round bottom flask which was fitted with a rubber septum. Initiator (**1**, 0.52 mmol) and 2-(2-(2-methoxyethoxy)ethoxy)ethyl acrylate (34.9 mmol) were mixed together and degassed for 30 min, followed by the addition of the mixture to the round bottom flask using a needle while backfilling with N_2. The green reaction mixture was degassed for 15 min and placed in a 70 ºC oil bath for 18 h. After 18 h, the polymer was isolated and purified by dissolving in THF and filtering through a short plug of basic Al_2O_3. The resulting solution was concentrated *in vacuo* and then precipitated in cold hexanes (x 3) to remove unreacted monomer, decanting hexanes after each precipitation step. The solution was further dried in a vacuum oven to yield 40 % (mass yield) of a yellow viscous oil. (M_n = 13,000 g mol^{-1}, $Đ$ = 1.13). $POEG_2MA$ was synthesized following the same procedure with 2-(2-methoxyethoxy)ethyl methacrylate (M_n = 11500 g mol^{-1}, $Đ$ = 1.2)

Deprotection of Phthalimide endcapped Poly2-(2-(2-Methoxyethoxy)ethoxy)ethyl methacrylate ($POEG_3A$)

Phthalimidyl functionalized $POEG_3A$ (5 g, 0.38 mmol) was dissolved in 20 mL of THF in a round bottom flask, followed by the addition of 1 mL of hydrazine hydrate. The reaction was refluxed for 2 hours which resulted in the formation of a white precipitate (phthalhydrazide). The solution was centrifuged and the top layer was precipitated in THF and centrifuged (x 2) to remove residual phthalhydrazide. The top layer was concentrated *in vacuo* to yield a yellow viscous oil. Yield: 4.31g (86% by mass), M_n = 12,700 g mol^{-1}, $Đ$ = 1.15. Phthalimidyl functionalized $POEG_2MA$ was deprotected following the same procedure (88% yield, M_n = 12,100 g mol^{-1}, $Đ$ = 1.24).

Synthesis of $POEG_3A$ grafted Cellulose nanocrystals (*t*-CNC-g-$POEG_3A$)

t-CNC-g-$POEG_3A$ was synthesized following a previously published procedure for grafting polymers onto CNCs with minor modifications.[38] In short, *t*-CNC-COOH (200 mg, 0.191 mmol) were dispersed in DMF at 1 wt% via sonication and transferred into a round bottom flask. NHS (219 mg, 1.91 mmol) and DIC (240 mg, 1.91 mmol) were added to the reaction and allowed to stir for 15 min. Amine – functionalized $POEG_3A$ (3.22g, 12,700 g mol^{-1}, 0.215 mmol) was added to the suspension resulting in a light yellow color, which was placed in an oil bath at 70 ºC and allowed to stir for 48 h. The reaction was precipitated in diethyl ether and separated by centrifuging. To ensure efficient removal of unreacted polymer, the resulting solid was dispersed in THF followed by a repetitive sequence of: ultrasonication at 20% amplitude for 5 mins, centrifuging, decanting of the top solution and addition of excess THF. This sequence was repeated 5 times until the top solution was clear, suggesting efficient removal of unreacted polymer. *t*-CNC-g-$POEG_3A$ was dialyzed in a 50/50 methanol:water solution for 24 h, and dried in a lyophilizer to

yield a light yellow fluffy solid. Kaiser tests on the dried *t*-CNC-g-$POEG_3A$ remained yellow, indicating the absence of free amines from unreacted polymer (Figure S6).[45] Final mass: (650 mg, ca. 70 wt% grafted polymer by mass). Following already established procedures,[40] conductometric titration was used to determine the charge density of the *t*-CNC-g-$POEG_3A$. In order to calculate the concentration of $–CO_2H$ moieties remaining on the CNCs a few assumptions were made. We assume that all *t*-CNCs are recovered after purification and as such, 30 wt.% of the *t*-CNC-g-$POEG_3A$ is the *t*-CNCs and 70 wt.% is the grafted polymer (based on mass yield obtained). Based on calculations from the conductometric titration (equation 1), a charge density of 800 mmol/kg of residual carboxylic acid groups is obtained which would suggest we have ca. 154 mmol/kg of carboxylic acid converted during polymer grafting (ca. 16%).

$$\text{Charge density}\left(\frac{\text{mmol}}{\text{kg}}\right) = \frac{\Delta V\ (\text{mL}) \times C(\text{M})}{\text{m (kg)}} \qquad (1)$$

Where ΔV obtained from conductometric titrations = 0.6 mL, C is the concentration of NaOH used for conductometric titrations = 0.01M, and m is the mass of *t*-CNCs used = 7.5 mg.

t-CNC-g-$POEG_2MA$ was synthesized in similar fashion (M_n of $POEG_2MA$ = 12,100 g/mol) yielding a final mass of 550mg (63 wt% grafted polymer by mass).

_t_-CNC-g-$POEG_y$(M)A Nanocomposites

t-CNC-g-$POEG_y$(M)A were sonicated in DMF (5 mg/mL) and PVAc was dissolved in DMF (50 mg/mL). For example, 15 wt% nanocomposites were prepared by combining 75 mg of *t*-CNC-g-$POEG_y$(M)A (15 mL of DMF dispersion) and 425 mg of PVAc (8.5 mL of DMF solution) in a vial before transferring into Teflon® petri dishes. The dishes were placed into a vacuum oven at 45 ºC for 7 days. The resulting composite was compression molded between spacers in a Carver

laboratory press at 85 ºC at 3500 psi for 5 min (x 2) to yield 200-300 μm flexible thin nanocomposite films.

Aqueous Swelling

Dried specimens in the form of rectangular films were weighed using a four-digit balance and then immersed in deionized water at 37 °C. The samples were removed every 24 h, gently blotted using filter paper, weighed and immediately re-immersed in deionized water. Swelling measurements were conducted for 5 days to ensure equilibrium swelling weights and were carried out in triplicate. The water uptake (WU) was determined from the relative increase in weight of the specimens following equation 2.

$$WU = \frac{M_t - M_0}{M_0} \times 100 \qquad (2)$$

where M_t and M_0 are the mass of the specimens after water immersion for a certain period of time (t) and before immersion in deionized water respectively.

Details of the Percolation Model[42,43,46]

According to the percolation model, the modulus of the composite E´ can be expressed by:

$$E' = \frac{(1-2\psi+\psi X_r)E_s' E_r' + (1-X_r)\psi E_r'^2}{(1-X_r)E_r' + (X_r-\psi)E_s'} \qquad (3)$$

where E'_s is the tensile storage modulus of the soft matrix phase, and E'_r and X_r are the tensile storage modulus and the volume fraction of the rigid filler phase, respectively. Ψ is the percolation volume fraction of filler particles that participate in the load transfer, which according to the percolation theory is:

$$\psi = X_r \left(\frac{X_r - X_c}{1 - X_c} \right)^{0.4} \qquad (4)$$

where X_c with $X_r \geq X_c$ and $X_c \geq 0.7/A_r$ (A_r is the aspect ratio of the nanofibers) is the critical filler volume fraction needed for percolation.

Mechanical parameters used in Percolation Model:

E' – tensile storage modulus above T_g determined by DMA at 80 °C for PVAc composites.

E'_r – of the neat *t*-CNC-POEG$_y$(M)A film after being dried above LCST as determined by DMA (See Figure S9). E'_r = 2GPa.

E'_s – of the matrix as determined by DMA at 80 °C (See Figure S9). $E'_{s\,(PVAc)}$ = 0.3MPa.

X_r – is the volume fraction of the CNCs in the matrix and is controlled experimentally.

X_c – critical volume fraction of the cellulose nanofiber (=0.007) defined as $0.7/A_r$.[47]

Small – Angle Neutron Scattering (SANS)

SANS was performed at the National Institute of Standards & Technology Center for Neutron Research (NCNR, Gaithersburg, USA) on the NGB 30m SANS instrument. Scattered neutron intensities were measured at sample-to-detector distances of 1m, 4m, and 13m, and radially averaged yielding intensity as a function of scattering variable $q=(4\pi/\lambda)\sin(\theta/2)$, where θ is the scattering angle. The neutron wavelength λ=4Å. Measurements were taken at 20, 30, 40, and 60 ˚C. Samples were allowed to equilibrate for 30 minutes at each temperature prior to beginning a measurement. SANS data were fit according to a general Guinier-Porod (GP) model,[48]

$$I(q)=\begin{cases}\dfrac{G}{q^s}\exp\left(\dfrac{-q^2R_g^2}{3-s}\right)+B & \text{for } q \leq q_1 \\ \dfrac{D}{q^d}+B & \text{for } q \geq q_1\end{cases}$$

The term at low q (*i.e.,* $q \leq q_1$) describes the shape of the objects in solution. For example, $s = 0$ implies that the objects are globular, whereas $s = 1$ implies the presence of rod-like objects. R_g is the radius of gyration for the entire object in solution, *e.g.,* the bare *t*-CNCs or the *t*-CNCs and grafted polymers. The exponent d in the high q term yields information on the conformation of the grafted polymer chains. For $d = 2$, the chains adopt ideal conformations. A value of $d = 3$ implies collapsed polymer chains. Thus, as T approaches the LCST, d is expected to increase in magnitude. The coefficients G and D are scale factors, and B is the incoherent neutron background.

Simulations

Energy Conserving Dissipative Particle Dynamics (EDPD)

Similar to the original form of DPD[25] the EDPD extension is a coarse-grained particulate method in which the motion of the particles follow Newton's equation of motion.[49] A modified velocity-Verlet[50] time integration algorithm is used to solve the equation of motion of the particles. In EDPD in addition to momentum conservation, the time evolution of the particles is performed conserving the energy in the system. The governing equations are:

$$\frac{dr_i}{dt} = v_i$$

$$\frac{dv_i}{dt} = F_i$$

Where r_i and v_i represent the position and velocity of the particles respectively. The total force acting on each particle is the summation of three main pairwise forces.

$$F_i = \sum_{i \neq j} F_{ij}^C + F_{ij}^D + F_{ij}^R,$$

Where F_{ij}^{C}, F_{ij}^{D}, and F_{ij}^{R} are the conservative, dissipative and random forces respectively. The conservative force is a soft repulsive potential that represents the interaction between the particles.

$$F_{ij}^{C} = a_{ij}(T)\omega_{C}(r_{ij})\mathrm{e}_{ij}$$

In non-isothermal conditions, the interaction potential is a function of the system's temperature. According to the previous literature,[51] in order to capture the compressibility of liquid water the following form of the repulsion parameter is used:

$$a_{ij}(\mathrm{T}) = 75\,\mathrm{k}_{B}\,T/\rho$$

Where k_B is the Boltzmann number, T is the temperature and ρ is the number density of the particles. $\omega_{C}(r_{ij}) = (1-\mathrm{r}_{ij}/\mathrm{r}_{C})$ is a weight function that linearly decays with respect to the distance between the particles and eventually diminishes as the particles become farther than a certain cut-off value $(r_c = 1.0)$. The dissipative force dissipates the thermal energy from the system through the reduction of the relative velocity of the pair particles and the random force in the heat source for the system.

$$F_{ij}^{D} = -\gamma_{ij}\omega_{D}(r_{ij})(e_{ij}.v_{ij})e_{ij}$$

where γ_{ij} is the dissipation coefficient and $\omega_{D}(r_{ij})$ is the weight function for the dissipative force. Finally, the random force produces heat in the system through generating stochastic forces on the particles.

$$F_{ij}^{R} = \sigma_{ij}\omega_{R}(r_{ij})\xi_{ij}\Delta t^{-1/2}e_{ij}$$

Where σ_{ij} is the noise amplitude and ξ_{ij} is a Gaussian random number with zero mean and variance equal to unity. The dissipative and random forces together form a thermostat that conserves the temperature when the fluctuation-dissipation theorem is satisfied.

$$\sigma_{ij}^2 = \frac{4\gamma k_B T_i T_j}{T_i + T_j}$$

$$\omega_D(r) = \omega_R^2(r) = (1 - \mathrm{r}/\,\mathrm{r}_C)^2$$

DPD has been extended to an energy conserving form known as EDPD[49,24] that can treat non-isothermal phenomena.[26] In EDPD in addition to its momentum, each particle is associated with an internal energy whose time evolution is calculated according to the following equation:

$$C_v \frac{dT_i}{dt} = q_i = \sum_{i \neq j} (q_{ij}^C + q_{ij}^V + q_{ij}^R)$$

where C_v is the thermal capacity of EDPD particles, T_i is the temperature and q_i is the heat flux between interacting particles. The main components of the net flux are the collisional q_{ij}^C, viscous q_{ij}^V and random q_{ij}^R heat flux.

$$q_i^C = \sum_{i \neq j} k_{ij} \omega_{CT}(r_{ij}) \left(\frac{1}{T_i} - \frac{1}{T_j}\right)$$

$$q_i^V = \frac{1}{2C_v} \sum_{i \neq j} \left\{ \omega_D(r_{ij}) \left[\gamma_{ij} (e_{ij}.v_{ij})^2 - \frac{(\sigma_{ij})^2}{m} \right] - \sigma_{ij} \omega_R(r_{ij}) (e_{ij}.v_{ij}) \xi_{ij} \right\}$$

$$q_i^R = \sum_{i \neq j} \beta_{ij} \omega_{RT}(r_{ij}) dt^{-1/2} \xi_{ij}$$

In collisional heat flux, k_{ij} represents the thermal conductivity $k_{ij} = C_v^2 k(T_i + T_j)/4k_B$, in which k corresponds to the heat friction coefficient (~ 0.001). β_{ij} determines the strength of the random flux and is related to the thermal conductivity of the particles according to:

$$\beta_{ij}^2 = 2k_B k_{ij}$$

Moreover, as shown below, the commonly used quadratic weight functions are employed for the collisional and random heat flux.

$$\omega_{CT}(r) = \omega_{RT}^2(r) = (1 - r/r_c)^2$$

Simulated System

Nano-rods are constructed by attaching rigid particles together ($N_r = 30$). The whole rod is considered as one body and the equation of motion is integrated considering rigid body dynamics. Nevertheless, the time evolution of the internal energy follows the equations showed in the previous section. The small distance between the consecutive beads, $d = 0.2r_c$, results in an increased value for density around the nano-rods and consequently prevents them from overlapping. Polymer chains are constructed using a bead spring potential connecting 10 EDPD beads together. The same spring potential is used for grafting the chains onto the nano-rods (5 chains are grafted on each rod). The grafting sites are fixed but the chains are allowed to move around the centerline of the rods. Initially, the polymer-grafted rods are randomly distributed in a polymer matrix (made out of 70 EDPD beads). A film of the nano-composite is generated in the middle of the calculation box (35*26*35 r_c^3). 5*10^4 solvent particles that are initially generated on

top and bottom of the box are allowed to penetrate through the film; however, boundary conditions do not permit neither the rods nor the polymer matrix to escape the film. Solvent particles represent water molecules, rods are assumed to be hydrophilic (as *t*-CNCs are very hydrophilic) and are grafted with LCST polymer chains, and the matrix is slightly hydrophobic (as PVAc is also slightly hydrophobic). A Morse potential that can capture the hydrogen bonding effect is considered to be acting between the nano-rods. An imaginary bond is assumed to form between the neighboring rods; however, this bond will break when the distance between the rods exceeds a set cut-off value. $U_{rr} = K(1-\exp(-3.0(\mathrm{r}_{ij}-r_{eq}))^2)-7.0$, where $K = 10.0$ and $r_{eq} = 0.4r_c$. As stated previously, the repulsion parameter between the particles is a function of system temperature. For like particles $a_{ii}(\mathrm{T}) = 75\mathrm{k}_B T/\rho$ will give the compressibility of liquid water.[45] The excess repulsion between the unlike particles $a_{ij} = 75k_BT/\rho + \Delta a_{ij}(T)$ is related to the Flory-Huggins χ-parameter.[42] Here we consider a linear dependency on temperature for the excess repulsion between the unlike components $\Delta a_{ij}(T) = C_{ij}k_BT/\rho$ and the value of C_{ij} is set according to Table S1.

Following a method proposed by Li et al.,[26] in order to capture the LCST transition, the excess potential between the grafted chains and water particles is defined as $\Delta a_{ij} = A_0 + \frac{\Delta A}{1+\exp(-\tau.(T-T_C))}$, where T_C is the critical temperature and is set at 1.0. This function will induce an abrupt change in the interaction potential upon reaching above the critical temperature. In the equation shown above, $\tau = 300, \Delta A = 20$ *and* $A_0 = -10$.

Table S1 - Interaction potential between the system components

C_{ij}	Nano-rod	Grafted chain	Polymer Matrix	Solvent
Nano-rod	75.0	80.0	80.0	80.0
Grafted chain		75.0	90.0	80.0
Polymer Matrix			75.0	85.0
Solvent				75.0

Our aim is to monitor the thermo-sensitive structural changes using the described model. So after reaching the thermally equilibrium state ($2*10^5$ simulation time steps with $\Delta t = 0.01$), the system is heated up. Each EDPD particle is coupled with a thermal background whose temperature $T^B(t)$ is a linearly increasing function of the simulation time. Thus, depending on the temperature difference each EDPD particle obtains a heat flux from the background according to the following equation.

$$Q_i^S(t) = \lambda.\mathrm{C}_v.(T^B(t) - T_i(t))$$

where T_i is the particle temperature. As explained before, in the non-isothermal condition the conservative potential is a function of temperature and varies with simulation time. In our simulations the temperature is increased linearly with time (from 0.8 to 1.4). Figure S8 shows the temperature of the system that is calculated from the kinetic energy. Also, the interaction potential between the grafted chains and the solvent particles is calculated. As shown in Figure. S2c, the measured repulsive potential shows a dramatic change as the temperature increases above the LCST transition point $k_BT = 1.0$.

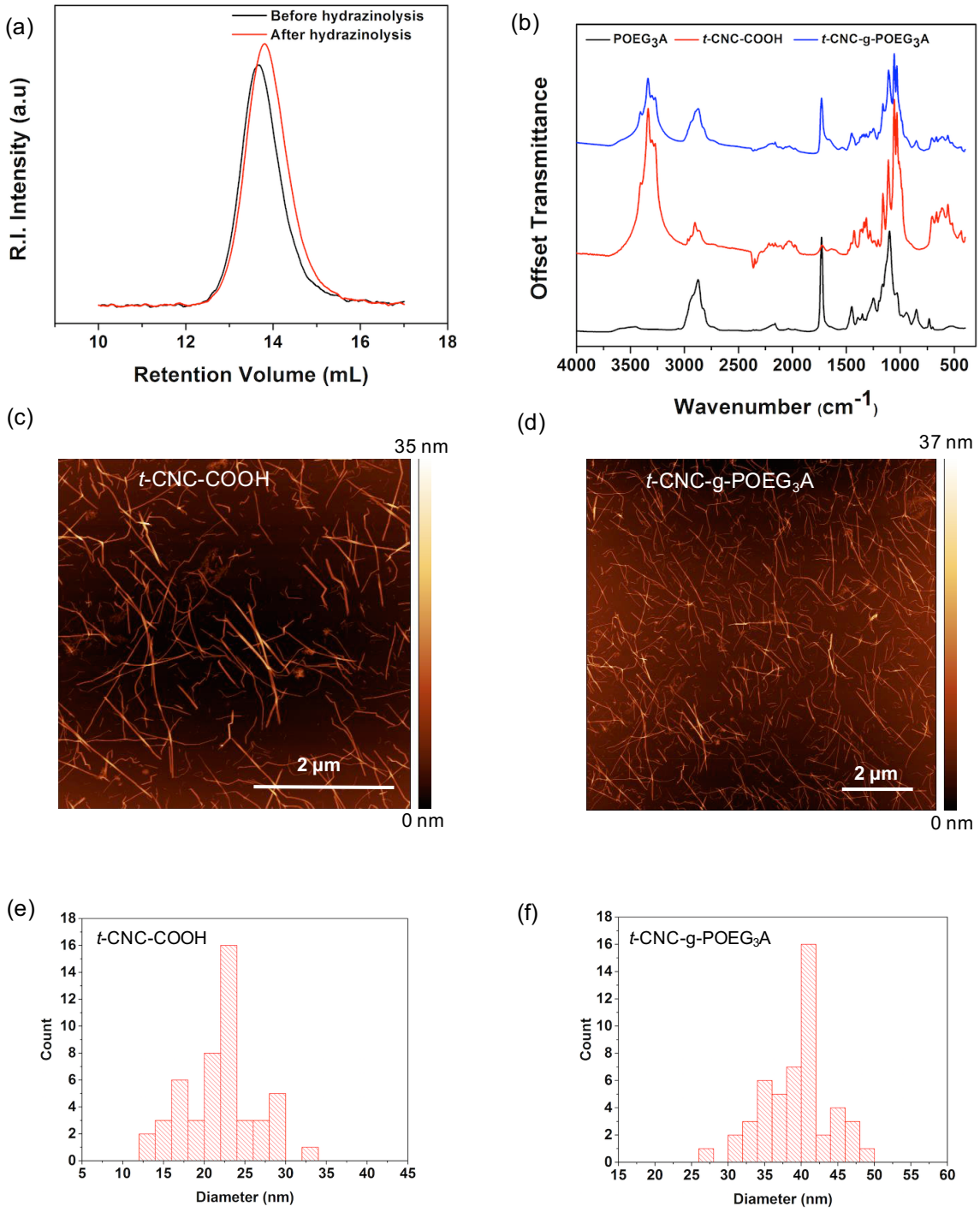

Figure S1. Characterization of the functionalized *t*-CNCs. (a) GPC of $POEG_3A$ (THF at 1mL/min) before (M_n=13,000 g/mol, $Đ$=1.13) and after (M_n=12,700 g/mol, $Đ$=1.15) hydrazinolysis (b) FTIR spectra of *t*-CNC-COOH, $POEG_3A$ and *t*-CNC-g-$POEG_3A$. AFM images of (c) *t*-CNC-COOH and (d) *t*-CNC-g-$POEG_3A$ and histograms (50 measurements each) of the diameter of the (e) *t*-CNC-COOH and (f) *t*-CNC-g-$POEG_3A$ fibers obtained from the AFM images.

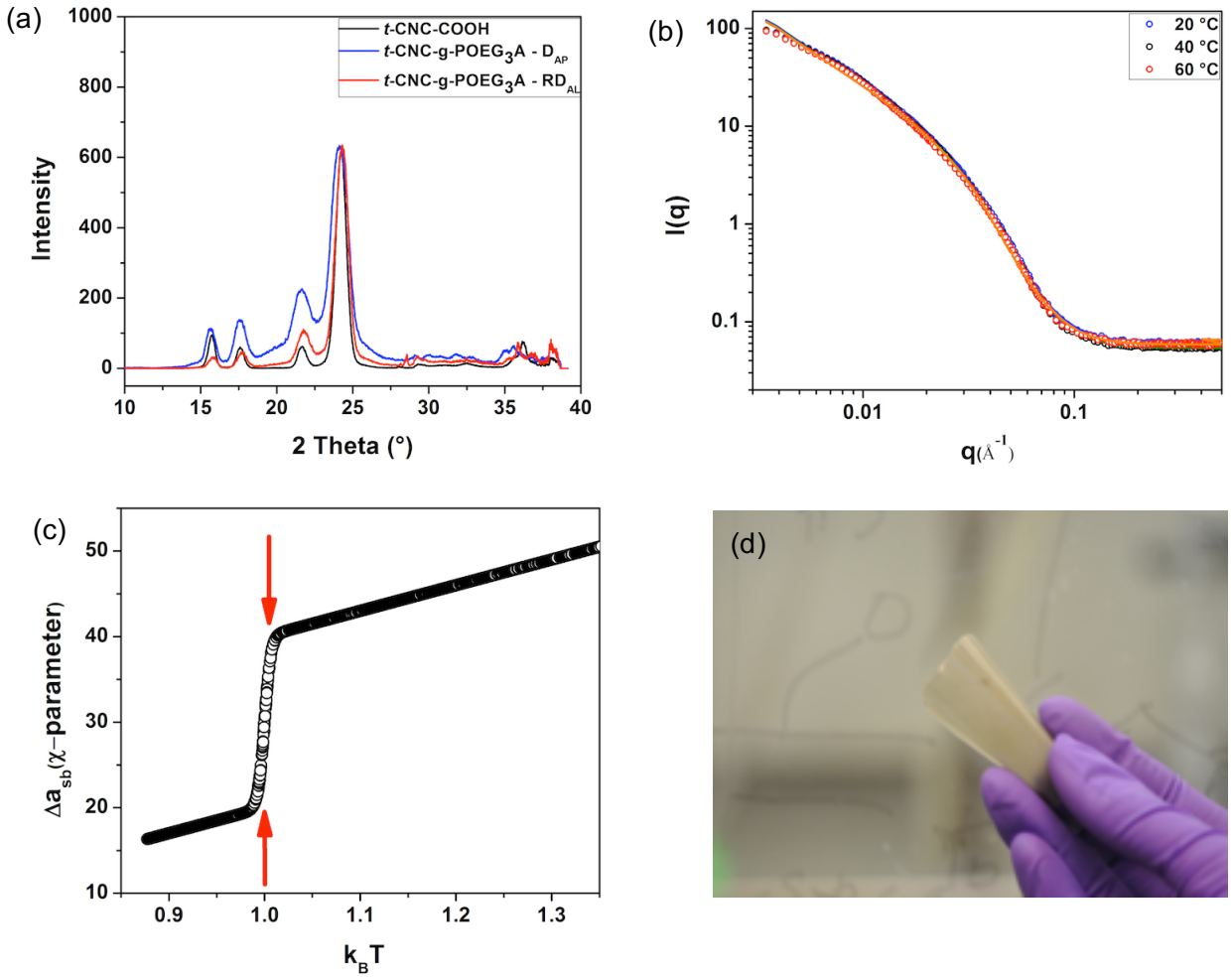

Figure S2. Characterization of the functionalized *t*-CNCs and interaction potential of EDPD model (a) Wide Angle X-ray Diffraction (WAXD) of of *t*-CNC-COOH, *t*-CNC-g-POEG$_3$A (dry as processed and re-dried above the LCST) (b) Small Angle Neutron Scattering profile of *t*-CNC-COOH as a function of temperature. (c) Interaction potential between grafted chains and solvent particles as a function of system's temperature (d) Flexible *t*-CNC-g-POEG$_3$A/PVAc nanocomposite

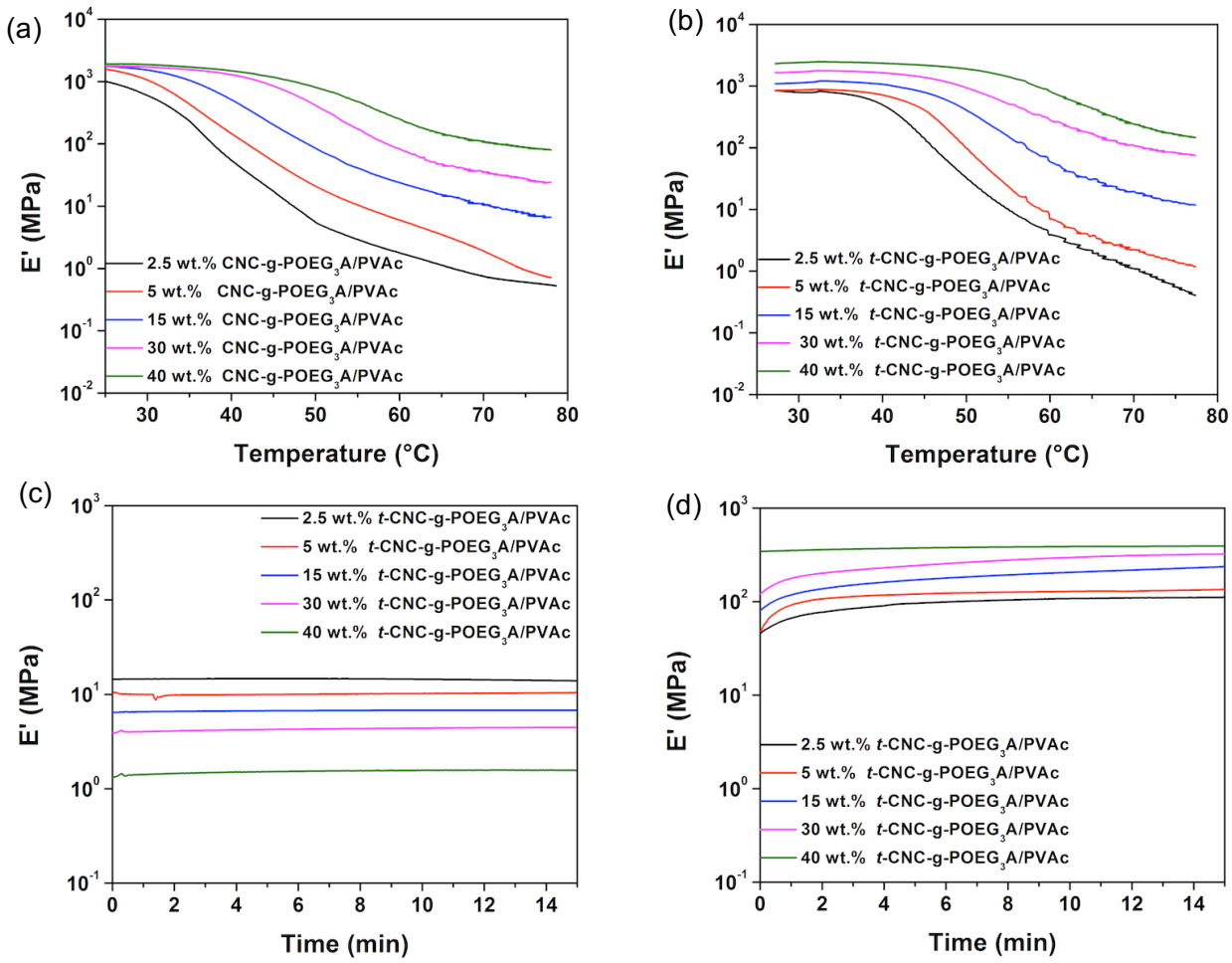

Figure S3. Characterization of *t*-CNC-g-POEG$_3$A/PVAc (composite set 1). DMA Temperature sweeps of the *t*-CNC-g-POEG$_3$A/PVAc nanocomposites (a) **1D$_{AP}$** and (b) **1RD$_{AL}$**. Representative data plots are shown. All experiments were run in triplicate. Wet time sweeps (performed at 0.1% strain, 0.01 N preload force, and a force track of 125% from 0-15 min) of *t*-CNC-g-POEG$_3$A/PVAc nanocomposites at (c) 30 °C and (d) 60 °C.

(a)

***t*-CNC-g-POEG$_3$A %wt/wt**	**PVAc %wt/wt**	**POEG$_3$A %wt/wt**	**CNC % wt/wt**	**% Water Uptake (30°C water)**	**% Water Uptake (60°C water)**
2.5	97.5	1.75	0.75	9.2 ± 1.3	6 ± 1.5
5	95	3.5	1.5	25.1 ± 1.9	15.1 ± 1.1
15	85	10.5	4.5	45.4 ± 3	23.4 ± 2.8
30	70	21	9	78 ± 2.6	42.9 ± 3.2
40	60	28	12	90.3 ± 3.1	58.7 ± 2.2

(b)

***t*-CNC-g-POEG$_3$A %wt/wt**	**E′ (MPa) Dry as-processed (1D$_{AP}$)**	**T$_g$ (°C) Dry as-processed (1D$_{AP}$)**	**E′ (MPa) (30°C water) (1W$_{BL}$)**	**T$_g$ (°C) Wet (1W$_{BL}$)**	**E′ (MPa) (60°C water) (1W$_{AL}$)**	**E′ (MPa) Re-dried Above LCST (1RD$_{AL}$)**	**T$_g$ (°C) Redried Above LCST (1RD$_{AL}$)**
2.5	720 ± 215	39.9	14 ± 0.09	19.7	100.1 ± 21.1	850 ± 320	41
5	633 ± 280	38.3	8.4 ±0.34	18.2	131.9 ± 23.8	863 ± 140	42
15	1000 ± 172	39.9	4.2 ±0.22	15.6	201.6 ± 16	1531 ± 266	41
30	1597 ± 386	40	1.9 ±0.45	N.D.	247.6 ± 22.9	1930 ± 312	42
40	1752 ± 330	40.9	0.84 ± 0.09	N.D.	320.1 ± 14.5	2815 ± 492	43

Table S2. Data for *t*-CNC-g-POEG$_3$A/PVAc (a) Composition and water uptake for composite set **1**, *t*-CNC-g-POEG$_3$A/PVAc nanocomposites (b) Glass transition temperature (T$_g$) and tensile storage modulus (E′) for composite set **1**. The modulus values under different conditions: dry as-processed (**1D$_{AP}$**, Dry As-Processed), soaked in below LCST water for 3 days (**1W$_{BL}$**, Wet Below LCST), placed in above LCST water (60°C) for 1 hour (**1W$_{AL}$**, Wet Above LCST) and re-dried above LCST (70°C) (**1RD$_{AL}$**, Re-dried Above LCST). T$_g$ data for *t*-CNC-g-POEG$_3$A/PVAc composites determined by DSC. All samples were run under a flowing nitrogen atmosphere and were heated and cooled at a rate of 10 ºC/min through the temperature range of -60 to 80°C. The glass transition temperatures were determined by taking the midpoints of the stepwise change in the heat flow signal from the heating and cooling traces. T$_g$ of the wet 30 and 40 wt% was not observed presumably as it is hidden by the T$_m$ of the water.

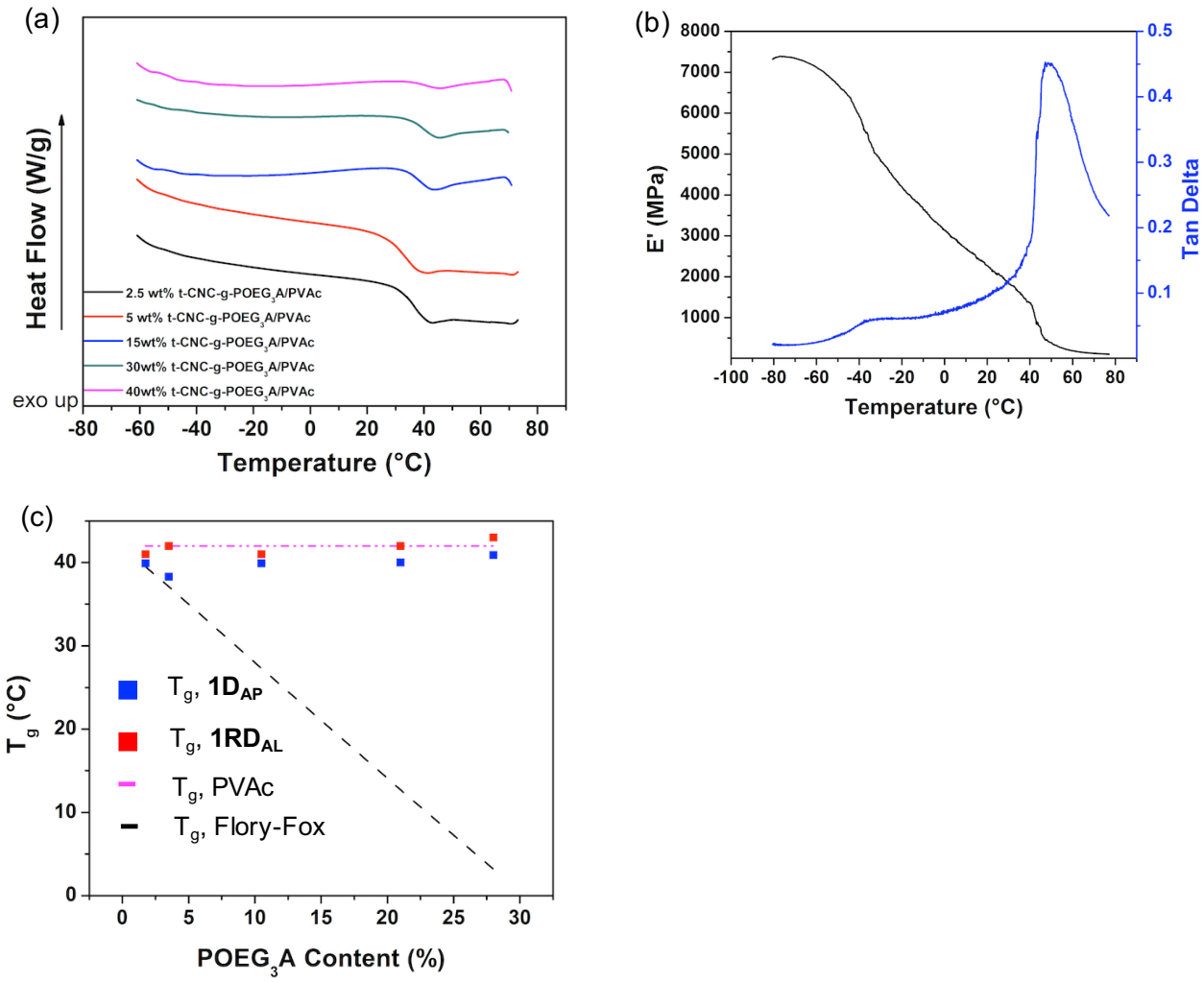

Figure S4. Characterization of *t*-CNC-g-POEG$_3$A/PVAc (composite set 1). (a) DSC curves showing no significant change in the T_g of the various nanocomposites with different *t*-CNC-g-POEG$_3$A content. (b) DMA temperature sweep of 40 wt% *t*-CNC-g-POEG$_3$A/PVAc showing a phase separated composite. (c) T_g data of composite films Dry As-Processed (**1D$_{AP}$**) and Re-Dried Above LCST (**1RD$_{AL}$**) determined by DSC (black dotted line and pink dotted line represents the Flory-Fox equation data and the T_g of PVAc respectively). The T_g's were determined from the stepwise change in the heat flow signal from the heating traces.

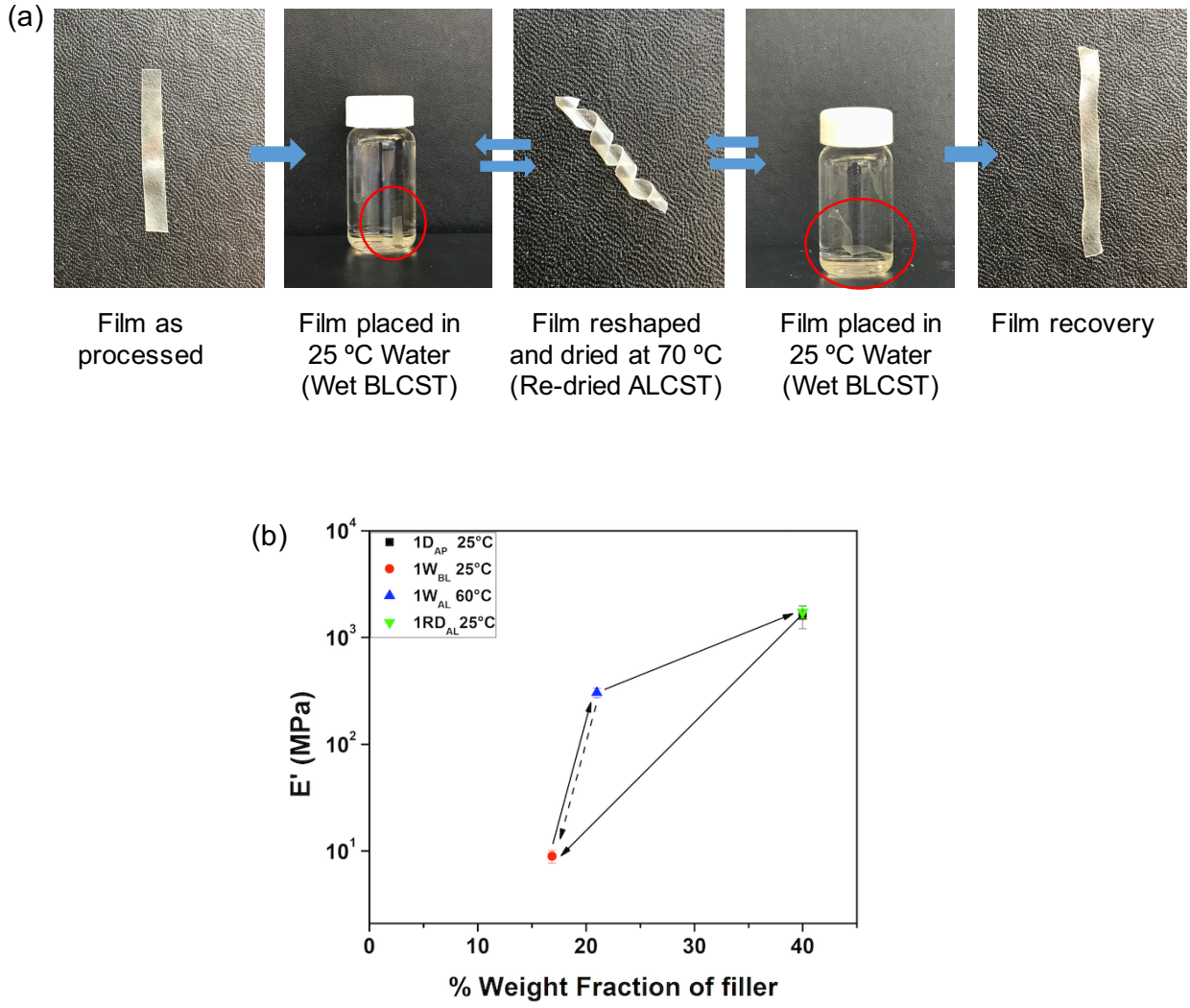

Figure S5. Additional Data on the *t*-CNC-POEG$_3$A/PVAc (composite set 1). (a) Images of *t*-CNC-POEG$_3$A/PVAc composite placed in 25°C water (BLCST), reshaped into a spiral and dried above LCST (70°C), placed back in 25°C water (BLCST) causing it to return to its original shape. **(b)** Tensile storage modulus (E′) under different conditions in salt solution: dry-as-processed (**1D$_{AP}$**, Dry-As-Processed), soaked in below LCST Earle's balanced salt solution for 3 days (**1W$_{BL}$**, Wet Below LCST), placed in above LCST Earle's balanced salt solution (60°C) for 1 hour (**1W$_{AL}$**, Wet Above LCST) and re-dried above 60°C (**1RD$_{AL}$**, Re-dried Above LCST).

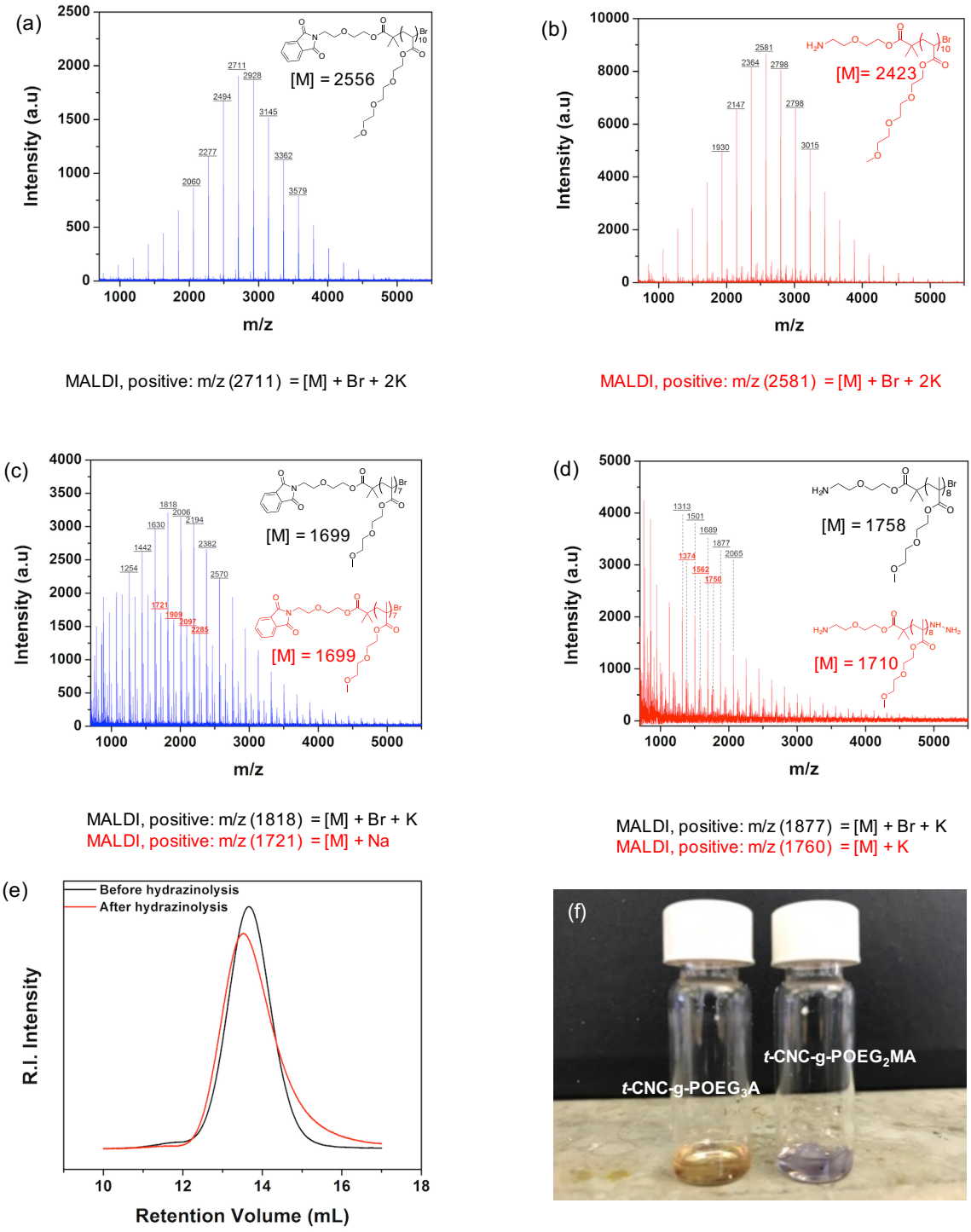

Figure S6. Matrix Assisted Laser Desorption/Ionization (MALDI). (a) Phthalamide protected end group of (a) $POEG_3A$ and (c) $POEG_2MA$. Deprotection of phthalamide protected (b) $POEG_3A$ and (d) $POEG_2MA$ using hydrazine. (e) GPC of $POEG_2MA$ (M_n=11500 g/mol, Đ=1.2) (f) Kaiser tests of t-CNC-g-$POEG_3A$ and *t*-CNC-g-$POEG_2MA$

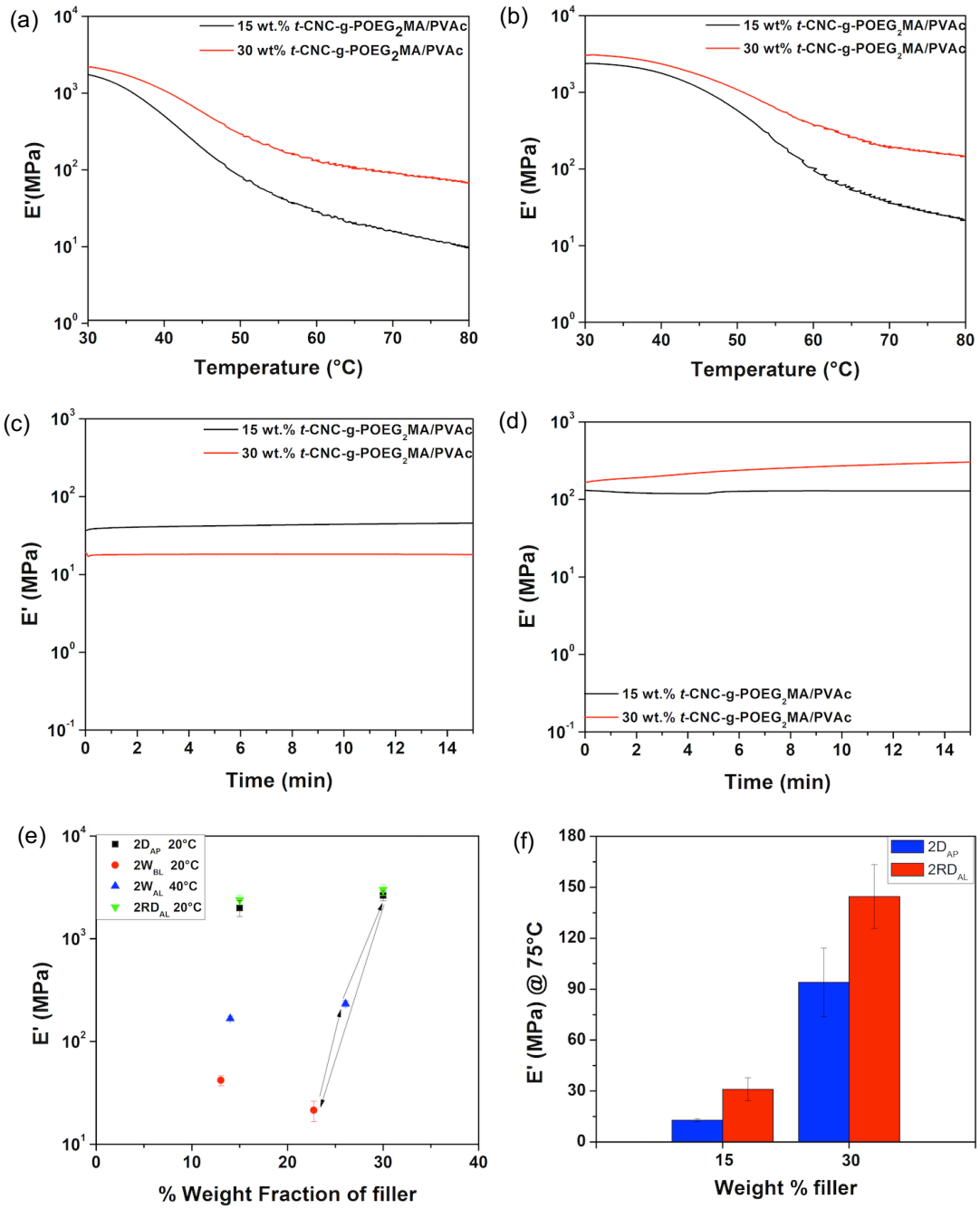

Figure S7. Additional Data on the *t*-CNC-g-POEG$_2$MA/PVAc (composite set 2). DMA Temperature sweeps of the *t*-CNC-g-POEG$_2$MA/PVAc nanocomposites (a) **2D$_{AP}$** and (b) **2RD$_{AL}$**. Representative data plots are shown. All experiments were run in triplicate. Wet time sweeps (performed at 0.1% strain, 0.01 N preload force, and a force track of 125% from 0-15 min) of *t*-CNC-g-POEG$_2$MA/PVAc nanocomposites at (c) 20°C and (d) 40°C. (e) DMA of *t*-CNC-POEG$_2$MA/PVAc composites dry as-processed (**2D$_{AP}$**), soaked in below LCST water for 3 days to equilibrium (**2W$_{BL}$**) and placed in above LCST water (40°C) for 1 hour (**2W$_{AL}$**) and re-dried above LCST (**2RD$_{AL}$**). (f) Storage Modulus of **2D$_{AP}$** and **2RD$_{AL}$** above glass transition temperature of the nanocomposites (75°C).

(a)

***t*-CNC-g-POEG$_2$MA %wt/wt**	**PVAc %wt/wt**	**POEG$_2$MA %wt/wt**	**CNC %wt/wt**	**% Water Uptake (20ºC water)**	**% Water Uptake (40ºC water)**
15	85	9.5	5.5	15 ± 1.9	7 ± 1.5
30	70	18.9	11.1	32.4 ± 2	15.2 ± 2.1

(b)

***t*-CNC-g-POEG$_2$MA %wt/wt**	**E´ (MPa) Dry as-processed ($3D_{AP}$)**	**E´ (MPa) (20°C water) ($3W_{BL}$)**	**E´ (MPa) (40°C water) ($3W_{AL}$)**	**E´ (MPa) Re-dried Above LCST ($3RD_{AL}$)**
15	1994.5 ± 351	41.9 ± 4.7	167.4 ± 9.5	2398.2 ± 254
30	2627.8 ± 285	21.4 ± 4.8	233.4 ± 16	3001.28 ± 361

Table S3. Data for *t*-CNC-g-POEG$_2$MA/PVAc (a) Composition and water uptake for composite set **2**, *t*-CNC-g-POEG$_2$MA/PVAc nanocomposites (b) Tensile storage modulus (E′) for composite set **2**. The modulus values under different conditions: dry as-processed (**$2D_{AP}$**, Dry As-Processed), soaked in below LCST water for 3 days (**$2W_{BL}$**, Wet Below LCST), placed in above LCST water (40°C) for 1 hour (**$2W_{AL}$**, Wet Above LCST) and re-dried above LCST (70°C) (**$2RD_{AL}$**, Re-dried Above LCST).

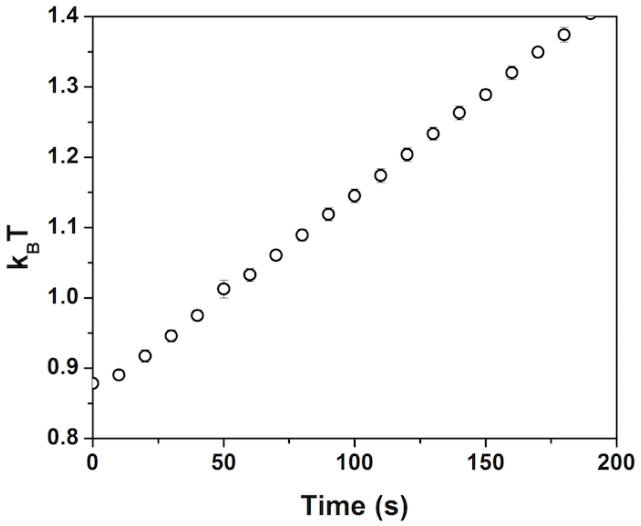

Figure S8. Additional Data on the simulation of the temperature responsive system. Temperature evolution versus time verifies the heating mechanism of the system determined from the kinetic energy of the particles.

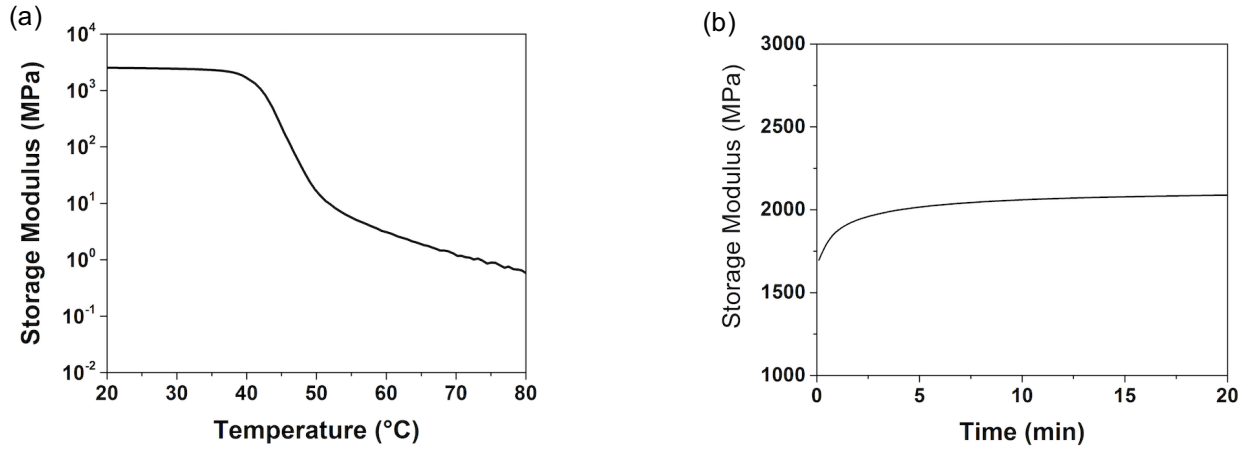

Figure S9. Additional experimental data used for the percolation model. (a) DMA temperature sweep of pure PVAc and (b) DMA time sweep (at 25°C) of neat dry *t*-CNC-g-POEG$_3$A after being wet and then dried above the LCST.

References

44. Belton, P., Tanner, S. & Cartier, N. High-resolution solid-state carbon-13 nuclear magnetic resonance spectroscopy of tunicin, an animal cellulose. *Macromolecules* **1989**, 22**,** 1615–1617

45. Kaiser, E., Colescott, R. L., Bossinger, C. D. & Cook, P. I. Color test for detection of free terminal amino groups in the solid-phase synthesis of peptides. *Analytical Biochemistry* **1970**, 34, 595-598

46. Ouali, N.; Cavaille, J.Y.; Perez, J. Elastic, viscoelastic and plastic behavior of multiphase polymer blends. *Plast. Rubber Compos. Process. Appl.* **1991**, 16, 55–60.

47. Favier, V., Dendievel, R., Canova, G., Cavaille, J. Y. & Gilormini, P. Simulation and modeling of three-dimensional percolating structures: Case of a latex matrix reinforced by a network of cellulose fibers. *Acta Mater.* **1997**, 45, 1557–1565.

48. Hammouda, B. A new Guinier-Porod model. *J. Appl. Cryst.* **2010**, 43, 716-719.

49. Español, P. Dissipative particle dynamics with energy conservation. *Europhys. Lett.* **1997**, 40, 631–636.

50. Groot, R. & Warren, P. Dissipative particle dynamics: Bridging the gap between atomistic and mesoscopic simulation. *J. Chem. Phys.* **1997**, 107, 4423–4435.

51. Groot, R. D. & Rabone, K. L. Mesoscopic Simulation of Cell Membrane Damage, Morphology Change and Rupture by Nonionic Surfactants. *Biophys. J.* **2001**, 81, 725–736.